

Thermoanalytical characterization of carbon/carbon hybrid material, Apple Woodceramics

Riko Ozao^{a,*}, Yuko Nishimoto^b,
Wei-Ping Pan^c, Toshihiro Okabe^d

^a SONY Institute of Higher Education, Atsugi, Kanagawa 243-8501, Japan

^b Kanagawa University, Department of Chemistry, Hiratsuka, Kanagawa 259-1295, Japan

^c Western Kentucky University, Department of Chemistry, 1 Big Red Way, Bowling Green, KY 42101, USA

^d Aomori Industrial Research Center, Environmental Technology Div., 4-11-6, Daini-onyamachi, Aomori 030-0113, Japan

Received 9 September 2005; received in revised form 18 October 2005; accepted 18 October 2005

Abstract

Woodceramics, a carbon/carbon composite of plant-originated carbon reinforced by glassy carbon from phenolic resin, was prepared from apple pomace at carbonizing temperatures of 1073 K (AWC800) and 1473 K (AWC1200), and characterized by thermoanalytical methods and X-ray diffraction (XRD). Simultaneous differential scanning calorimetry (DSC) and thermogravimetric (TG) showed complicated overlapping reactions similar to those of coal. The initial temperature of pyrolysis was obtained by fitting logistic functions to observed TG data. The results suggested that AWC1200 contained more volatile matter than AWC800. In an inert atmosphere, complicated devolatilization takes place. In an oxidizing atmosphere, thermal change occurs roughly in four steps: desorption of physically adsorbed matter; pyrolysis into aliphatic and aromatic fragments; ignition; combustion of char. The oxidation resistance of AWC1200 was superior to AWC800.

© 2005 Elsevier B.V. All rights reserved.

Keywords: Woodceramics; Pyrolysis; Combustion; TG; Curve separation; Accelerated deterioration test; Kinetics; Environmentally benign; Activation energy

1. Introduction

Woodceramics are carbon–carbon composite materials consisting of naturally occurring biologically originated amorphous carbon reinforced by glassy carbon generated from resin. They are porous composites made by impregnating wood or woody materials with a thermosetting resin such as phenol resin, and then carbonizing the material in a vacuum furnace [1]. Woodceramics enable use of various types of waste cellulosic materials [2–5]. Woodceramics are resistant to higher temperatures than the original wood, and because it is porous, the density is normally about 1.0 Mg m^{-3} , i.e., about the same as that of epoxy resins or polyethylene resins, about one-third that of widely used ceramics such as alumina. Physical properties of Woodceramics differ depending on the starting material and carbonizing temperature. However, it is now well established that Wood-

ceramics based on medium-density fiberboard of satisfactory strength (3.1 GPa Young's modulus; 24 MPa fracture strength) can be obtained by carbonizing at 1073 K or higher [6].

Minimal data on thermal properties [7,8] are reported on Woodceramics. The authors have reported thermogravimetry–differential thermal analysis/mass spectrometry (TG–DTA/MS) results on Woodceramics based on apple pomace (hereafter referenced simply as “Apple Woodceramics”) [3] prepared by carbonizing at different temperatures (1073 and 1473 K). The material showed favorable properties for use as gas adsorbents [5], friction materials and others. Since Woodceramics is believed to be a porous carbon composite consisting of cellulose- and lignin-originated carbon reinforced by the three-dimensional network of aromatic clusters generated by heating phenolic resin [2], similarities with coal are found [6].

An object of the present study is to characterize the thermal change of apple WC in further detail, find the difference between the phases formed by carbonizing at different temperatures, and to show quantitatively the difference in thermal and oxidation resistance of apple WC.

* Corresponding author. Fax: +81 46 250 8936.
E-mail address: ozao@aoni.waseda.ac.jp (R. Ozao).

2. Experimental

2.1. Samples

Samples of apple WC were obtained by mixing commercially available Apple Fiber (Nichiro Corporation) with phenolic resin BELLPEARL S890 (product of Kanebo, Ltd.) at a ratio of 6:4 (by mass) and carbonizing at 1073 K (AWC800) and 1473 K (AWC1200). The samples were 250 μm or less in granularity.

2.2. X-ray diffraction (XRD)

XRD patterns of the samples were obtained with a Bruker MF18XH222 diffractometer (Cu $K\alpha_1$, 35 kV/200 mA), at a scanning rate of 5°min^{-1} over an angle range of $10\text{--}100^\circ$ (2θ), with $K\alpha_2$ diffractions removed.

2.3. Simultaneous DSC–TG (SDT)

Differential scanning calorimetry (DSC) was performed simultaneously with thermogravimetric (TG) analysis with a simultaneous differential scanning calorimeter–thermogravimetric analyzer SDT2960 (TA Instruments) of about 10–15 mg each of samples in the temperature range of from RT to 1273 K at a heating rate of 2, 5, 10 and 20 K min^{-1} . The measurements were carried out under air flow of 100 ml min^{-1} Airgas Compressed Air (breathing grade), Type I, Grade D, 21% O_2 certified), and under dry nitrogen gas flow (Airgas NI ED300 Nitrogen Extra Dry) at a rate of 100 ml min^{-1} . The thermal change of the sample was identified, and oxidation resistance of the samples was evaluated from those results.

3. Results and discussion

3.1. XRD identification of the original samples

XRD patterns for AWC800 and AWC1200 are shown in Fig. 1. The broad peak ca. 26° (2θ) shows the aromatic ring stacking (so-called π band [9]); close to the 002 reflection for graphite, but showing presence of various layers differing in layer distance. The weaker peak ca. 43° (2θ) corresponds to about half the distance ($\approx 0.20 \text{ nm}$) of the d -spacing of peak ca. 26° ($\approx 0.40 \text{ nm}$). An increase in background level was observed

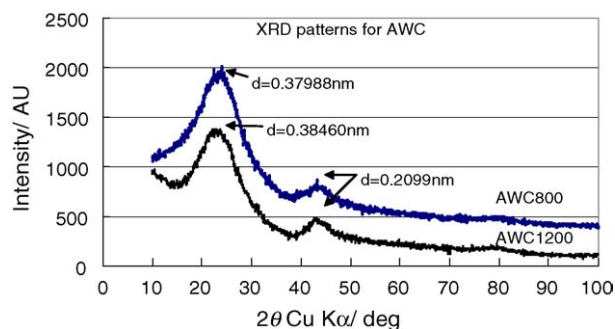


Fig. 1. XRD patterns of Apple Woodceramics sintered at 1073 K (AWC800) and at 1473 K (AWC1200).

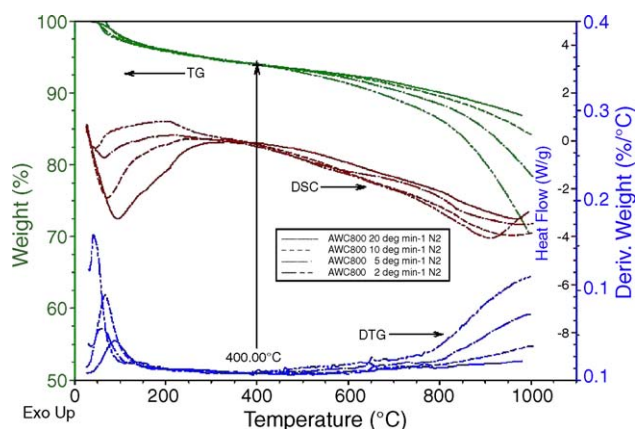


Fig. 2. TG, DSC and derivative TG (DTG) curves for AWC800 obtained in N_2 gas flow of 100 ml min^{-1} and at heating rates of 2, 5, 10 and 20°min^{-1} .

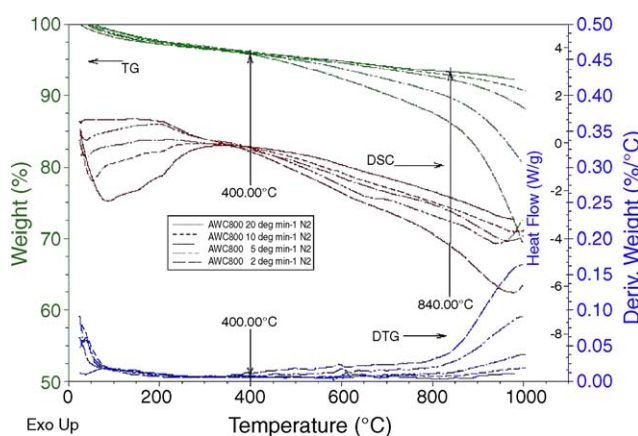


Fig. 3. TG, DSC and derivative TG (DTG) curves for AWC1200 obtained in N_2 gas flow of 100 ml min^{-1} and at heating rates of 2, 5, 10 and 20°min^{-1} .

for AWC1200 for 2θ angles lower than 15° . This might be attributed to the increase in number of turbostratic crystallites as explained by Kercher and Nagle [10].

3.2. Thermal change observed by TG–DSC (SDT) in nitrogen and air

In Figs. 2 and 3 are shown the TG, DSC and derivative TG (DTG) curves for AWC800 and for AWC1200, respectively, recorded at different heating rates. The mass loss results are summarized in Tables 1 and 2. For reference, data for AWC1200 heated at a rate of 1°min^{-1} are included in Fig. 2 and Table 2. For both samples, the mass loss percentage at temperatures lower

Table 1
TG results for AWC800 in inert atmosphere (in 100 ml min^{-1} N_2 gas flow)

| | Mass loss (%) at different heating rates | | | |
|------------|--|---------------------------|----------------------------|----------------------------|
| | 2°min^{-1} | 5°min^{-1} | 10°min^{-1} | 20°min^{-1} |
| RT–473 K | 7.27 | 4.60 | 6.37 | 3.98 |
| 473–873 K | 2.95 | 2.72 | 2.83 | 2.90 |
| 873–1273 K | 22.57 | 14.84 | 10.80 | 6.20 |
| Total | 32.79 | 22.16 | 20.00 | 13.08 |

Table 2
TG results for AWC1200 in inert atmosphere (in 100 ml min⁻¹ N₂ gas flow)

| | Mass loss (%) at different heating rates | | | | |
|------------|--|----------------------|----------------------|-----------------------|-----------------------|
| | 1° min ⁻¹ | 2° min ⁻¹ | 5° min ⁻¹ | 10° min ⁻¹ | 20° min ⁻¹ |
| RT–473 K | 3.05 | 3.69 | 3.92 | 4.07 | 2.54 |
| 473–873 K | 3.03 | 2.49 | 2.04 | 2.3 | 2.24 |
| 873–1273 K | 21.91 | 12.88 | 6.27 | 4.56 | 3.4 |
| Total | 27.99 | 19.06 | 12.23 | 10.93 | 8.18 |

than ca. 673 K seems to be heating-rate independent; i.e., it is about 10% for AWC800 and about 5% for AWC1200 in all heating rates, and this result is in conformity with previous results [3].

At temperatures up to ca. 473 K, from DSC and DTG in Figs. 2 and 3, it can be understood that endothermic reaction takes place with mass loss, and the peak temperatures of DTG and DSC shift to the higher temperature side with increasing heating rate. This suggests the reaction to be heating-rate dependent, and from our previous results obtained by TG–DTA/MS in flowing helium gas [3], it can be understood as desorption of inherent water and CO₂. The results for AWC1200 in this temperature range differ from those of AWC800 in that the amount desorbed is smaller than that of AWC800, thereby yielding peaks in a narrower temperature range.

In the temperature range ca. 473–673 K, the mass loss occurs monotonously for AWC800 and AWC1200, and the mass loss rate is the same for all the heating rates.

In the temperature range ca. 673–973 K for AWC800, the mass loss is higher for lower heating rates, and in temperatures higher than 973 K, the rate of mass loss increases considerably with decreasing heating rate. This temperature can be read as the inflection point in DTG curves. Moreover, with decreasing heating rate to 5° min⁻¹ or lower, a slight exothermic reaction appeared at temperatures higher than ca. 1173 K. As pointed out in the earlier studies [11–13] for lower heating rates, evolution of light gases and tar formation may be responsible for the mass loss, since evolution of CO₂ and low molecular fragments ($m/z=55$ and 78) was observed by mass spectroscopy [3]. At even higher temperatures, cross-linking may take place at the same time. In the earlier study [3] using MS for evolved gas analysis, the heating rate was high as 20° min⁻¹, and this might be the reason why no change was observed.

For AWC1200, similar results were observed at temperatures above 673 K (Fig. 3). However, the inflection point of DTG was observed at 1113 K; i.e., about 140° higher than the case for AWC800. Moreover, this temperature is in good agreement with that reported on coal pyrolysis [14].

In both samples of AWC800 and AWC1200, as stated above, additional exothermic reaction was observed at temperatures higher than 1173 K when heated at heating rates lower than 5° min⁻¹. This might represent combustion of char trapped inside the pores, because nitrogen gas flow still contains about 20 ppm oxygen.

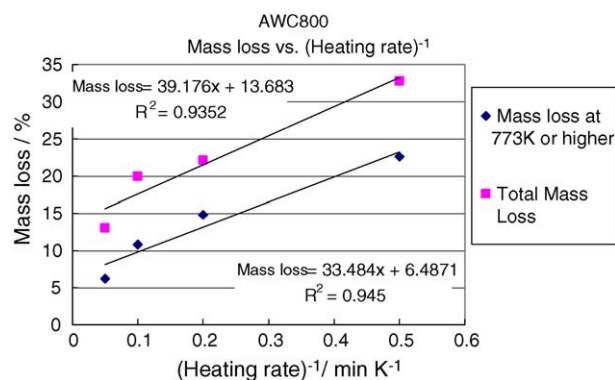


Fig. 4. Mass loss (fraction reacted) for AWC800 plotted against reciprocal of heating rate (where x in the inlay equation represents inverse of heating rate).

The mass loss in temperatures higher than 773 K increases with decreasing heating rate. An ordinary chemical reaction in which no overlapping or synergetic processes are involved, the following rate equation is generally applicable:

$$\frac{d\alpha}{dt} = f(\alpha) \cdot Z \exp\left(-\frac{\Delta E}{RT}\right) \quad (1)$$

where α represents the fraction reacted, t the time, $f(\alpha)$ the function of α not involving temperature, ΔE the activation energy, R the gas constant, Z the pre-exponential factor and T is the temperature.

Under the experimental condition of constant heating rate, temperature is proportional to time: $T = T_0 + Bt$, where B is the heating rate, and the following equation holds:

$$\frac{dT}{dt} = B \quad (2)$$

Thus, by substituting (2) into (1), and by integration, the following equation can be obtained:

$$\ln(\alpha) = \frac{1}{B} \cdot \frac{R}{\Delta E} Z \exp\left(-\frac{\Delta E}{RT}\right) \quad (3)$$

Since the activation energy should be constant for the entire reaction, because $f(\alpha)$ is independent to temperature as stated above, the left-hand side of Eq. (3) becomes proportional to $1/B$ at a certain temperature T , for instance, let it be 1273 K in this case. Since the fraction reacted can be directly related to mass loss in percentage, the mass loss plotted against the reciprocal of heating rate may yield a linear relation if $\ln f(\alpha) \propto \alpha$, i.e., $f(\alpha) \propto \exp(\alpha)$ according to the following equation:

$$\ln(\alpha) = \left(\frac{1}{B}\right) \cdot \text{constant} \quad (4)$$

Figs. 4 and 5 show the relationship between $1/B$ and α for AWC1200 and AWC800, respectively. Excellent linear relationship is obtained for AWC1200, particularly for the mass loss in the temperature range higher than 773 K. Thus, in this case, the reaction mechanism in nitrogen gas flow may not change over the entire process. For AWC800, however, plots for higher heating rates deviate from those for lower heating rates. This suggests that the thermal process of AWC800 in nitrogen is different from that of AWC1200.

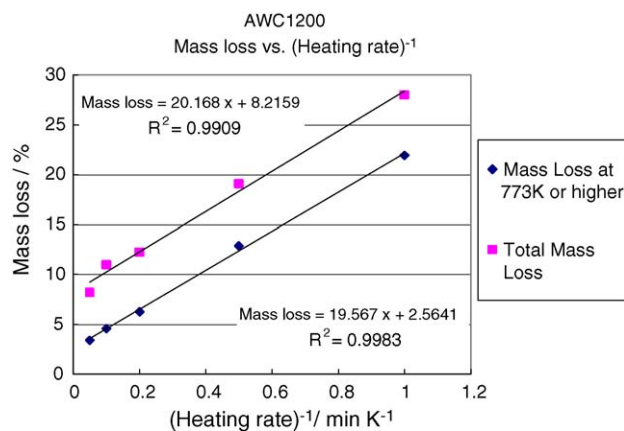


Fig. 5. Mass loss (fraction reacted) for AWC1200 plotted against reciprocal of heating rate (where x in the inlay equation represents inverse of heating rate).

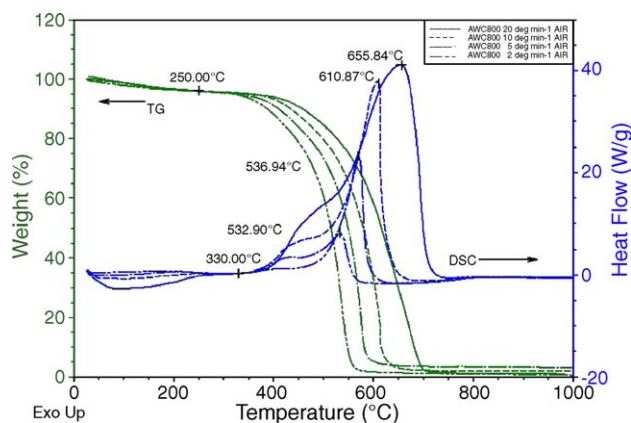


Fig. 7. TG and DSC curves obtained in air flow at different heating rates for AWC1200.

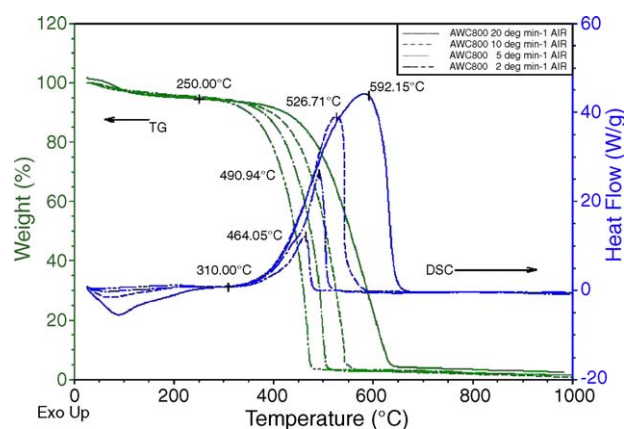


Fig. 6. TG and DSC curves obtained in air flow at different heating rates for AWC800.

Fig. 6 shows the TG, DSC and DTG curves for AWC800 obtained under air flow of 100 ml min^{-1} and at different heating rates of 2, 5, 10 and 20 K min^{-1} . It can be seen that the thermal change of apple WC in air proceeds in three stages. In the first stage from ambient to temperatures up to ca. 500 K, the mass loss is about 5%, which is attributed to the loss of physically adsorbed water or gaseous CO_2 as was the case for heating in nitrogen gas flow. This is in conformity with the cases reported on coal [14–18].

The second stage is sequential to the first stage and lasts in a temperature range of ca. 773–900 K. In this stage, it should be noted that the exothermic peak for all the heating rates initiate at temperatures about 60° higher than the initial temperature of mass loss. That is, the initial temperature of this exothermic reaction is not heating-rate dependent, but is almost the same for all heating rates. This provides evidence that volatile matter is first formed to evolve light gases as in the case of coals [14–16], and that the DSC exotherm represents ignition of volatile matters and successive combustion. The final temperature of this exothermic reaction is higher with increasing heating rate. Accordingly, in the second stage, ignition and successive combustion occurs while increasing the rate of pyrolysis. In the final stage at temperatures higher than ca. 773–900 up to 1273 K, a nearly constant and slight mass loss is observed.

The results obtained above for AWC800 are summarized in Table 3 together with those obtained for AWC1200. In Table 3, T_f represents the extrapolated onset for the end of mass loss. From the results obtained by peak integration of DSC curve, the heat generated in this temperature range is about 20 kJ g^{-1} , and is in good agreement with the value given for beech WC [2].

Fig. 7 shows the TG and DSC curves obtained in air flow at different heating rates for AWC1200. In this case again, three stages are observed in the TG curves similar to those obtained for AWC800. However, difference between AWC1200 and AWC800 is clearly discerned in the DSC curves. Exothermic

Table 3
TG results for AWC800 and AWC1200 in 100 ml min^{-1} air flow

| Heating rate ($^\circ \text{ min}^{-1}$) | Sample | T_e (K) | T_f (K) | Net mass loss, ($T_e - T_f$) (%) |
|--|---------|-----------|-----------|------------------------------------|
| 2 | AWC800 | 699.8 | 747.5 | 89.40 |
| | AWC1200 | 725.1 | 825.2 | 92.01 |
| 5 | AWC800 | 711.5 | 779.3 | 89.92 |
| | AWC1200 | 761.3 | 856.2 | 92.09 |
| 10 | AWC800 | 721.3 | 818.5 | 88.72 |
| | AWC1200 | 784.8 | 888.8 | 91.02 |
| 20 | AWC800 | 743.5 | 903.5 | 88.19 |
| | AWC1200 | 807.5 | 956.9 | 91.18 |

Table 4
Parameters for the logistic function fitting

| Parameters | Heating rate ($^{\circ}\text{min}^{-1}$) | | | |
|-------------------------|--|-----------|----------|-----------|
| | 2 | 5 | 10 | 20 |
| w_1 | 1.3572 | 1.28322 | 3.34977 | 0.636672 |
| a_1 | -0.595167 | -0.119182 | 11.9906 | 1.91189 |
| b_1 | 0.0169348 | 0.0560033 | 0.253841 | 0.317728 |
| w_2 | 3.78429 | 3.36007 | 0.485148 | 3.10339 |
| a_2 | 12.0852 | 12.2204 | 1.89038 | 12.3914 |
| b_2 | 0.0573827 | 0.1357 | 0.179869 | 0.491394 |
| w_3 | 6.50913 | 5.60931 | 6.38705 | 7.3659 |
| a_3 | 43.0746 | 47.9183 | 38.7231 | 24.0823 |
| b_3 | 0.174112 | 0.455738 | 0.69823 | 0.796906 |
| Residual standard error | 0.0396105 | 0.0319374 | 0.022808 | 0.0477972 |

peak is more distinctly observed at the beginning of the second stage (ca. 673–773 K) with decreasing heating rate, and an exotherm is also observed in the third stage with lowering heating rate. Those two effects have not been reported on any type of Woodceramics so far [3,7], because thermal analyses have been performed only on heating rates of $10^{\circ}\text{min}^{-1}$ or higher. However, these two effects were reported in coals [12–14]; the pre-reaction (exotherm) in the second stage is typically observed for lignite coals, which contain volatile matter for about 50%, and the slight exotherm in the third stage is attributed to the combustion of char. However, it is also known that pyrolysis, or devolatilization, occurs conjointly with oxidation and combustion [11].

3.3. Curve separation

Since pyrolysis, ignition of volatile matter and combustion were found to occur in parallel or conjointly with each other, an attempt was made to separate the overlapping reactions observed in TG curve of AWC1200 by assuming that the TG curve is composed of plural curves each expressed by logistic functions [19] as follows:

$$Y(t) = \sum_{i=1}^k w_i f(a_i + b_i t); \quad f(t) = \frac{e^t}{1 + e^t} \quad (5)$$

where $i = 1, 2, \dots, k$ represent different components from the mass loss process point of view, not necessarily different chemical compounds. From practical point of view, i is less than 4. Fitting of data to the logistic functions was performed by iterations and was evaluated by the residuals.

As a result, the data were fitted to logistic functions as follows:

$$Y(t) = w_1 \cdot \frac{\exp(a_1 - b_1 t)}{1 + \exp(a_1 - b_1 t)} + w_2 \cdot \frac{\exp(a_2 - b_2 t)}{1 + \exp(a_2 - b_2 t)} + w_3 \cdot \frac{\exp(a_3 - b_3 t)}{1 + \exp(a_3 - b_3 t)} \quad (6)$$

The parameters for Eq. (6) in separating each of the TG curves obtained in different heating rates are given in Table 4. For example, Fig. 8 shows observed TG curve fitted to a case obtained for a heating rate of 2°min^{-1} . The calculated curves are all in excel-

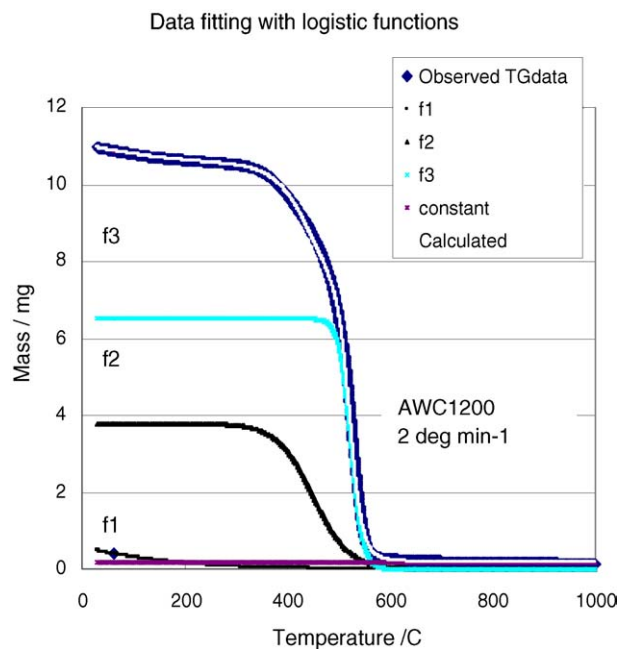


Fig. 8. TG curve fitted with logistic functions using parameters in Table 4.

lent agreement with the observed values, as can be evaluated by the small residual standard errors.

From the results above, the original TG curve is separated into four overlapping reactions. Thus, derivatives (Δ) of each curve were calculated, and the point at which the derivative Δ exceeded 0.00005 was read as the initial temperature of each mass loss curve. The results are summarized in Table 5.

By plotting the initial temperature T_i on the DSC–TG curves obtained in air and in nitrogen gas flow for the case of heating at 2°min^{-1} , it can be seen that T_i for f_2 indicates the temperature at which the ignition initiates; i.e., at this temperature and beyond, the TG curve obtained in inert gas departs from that obtained in air. Thus, the T_i obtained by the curve separation above provides the temperature at which pyrolysis is separated from ignition and combustion as pointed out by Pan and coworkers [14–16]. However, the meaning of T_i for f_3 is yet to be clarified. Moreover, the curve separation for AWC800 was found unfeasible up to this point.

3.4. Evaluation of oxidation resistance

In order to evaluate oxidation resistance by applying kinetic analysis, it is well known to employ accelerated lifetime testing based on Flynn and Wall [20] and Ozawa [21]. In this method, the

Table 5
Initial temperature T_i obtained by curve separation for each of the reactions

| T_i (K) | Heating rate ($^{\circ}\text{min}^{-1}$) | | | |
|-----------------|--|--------|--------|--------|
| | 2 | 5 | 10 | 20 |
| T_i for f_1 | 559.28 | 561.15 | 566.87 | 575.34 |
| T_i for f_2 | 721.86 | 722.65 | 723.70 | 759.65 |

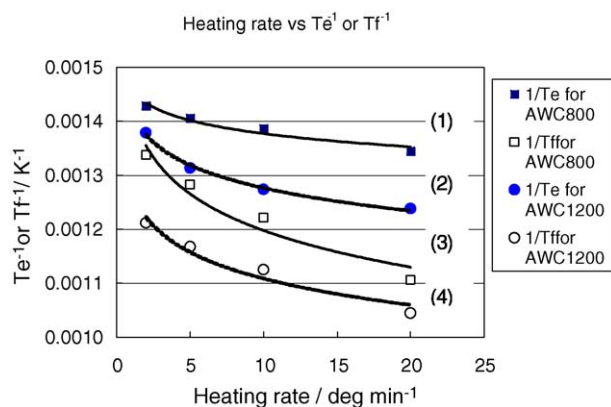


Fig. 9. Reciprocal of T_e and T_f for AWC800 and AWC1200, plotted with changing heating rate. (1) $T_e^{-1} = -4 \times 10^{-5} \ln(x) + 0.0015$ ($R^2 = 0.9513$); (2) $T_e^{-1} = -6 \times 10^{-5} \ln(x) + 0.0014$ ($R^2 = 0.9936$); (3) $T_e^{-1} = -1 \times 10^{-4} \ln(x) + 0.0014$ ($R^2 = 0.9417$); (4) $T_e^{-1} = -7 \times 10^{-5} \ln(x) + 0.0013$ ($R^2 = 0.9537$); where x represents heating rate.

reaction is described by Eq. (1). As stated before, it is required that the reaction is described by a function (although it may be model-free) over the entire temperature range considered.

The applicability of kinetic evaluation above was examined by plotting the reciprocal of T_e and T_f of the TG curves (given in Table 3) with respect to the heating rates. If the same rate function $f(\alpha)$ applies for all the heating rates, T_e may represent the temperature for the same conversion ratio α_1 , for instance, 0.05. Similarly, if the same rate function applies for all the heating rates, T_f may represent the temperature for the same conversion ratio α_2 , for instance, 0.95. Thus, at T_e or T_f , $f(\alpha)$ should be the same in case the same rate function is applicable. Accordingly, by rearranging Eq. (3), we obtain:

$$B = \frac{1}{\ln f(\alpha)} \cdot \frac{R}{\Delta E} Z \exp\left(-\frac{\Delta E}{RT}\right) \quad (7)$$

Since the pre-exponential factors (not only Z) should be constant at T_e and T_f , taking the logarithm of both sides yield:

$$\ln B = \text{constant} + \left(-\frac{\Delta E}{RT}\right) \quad (8)$$

In Fig. 9 are plotted the reciprocal of T_e and T_f for AWC800 and AWC1200 with changing heating rates. From the regression curves drawn in Fig. 8, it can be understood that T_e and T_f for AWC800 and AWC1200 fairly satisfies Eq. (8). Thus, although the reaction mechanism is still to be studied in detail, apparent activation energy and 60-min half-life temperature for AWC800 and AWC1200 obtained for 5% conversion are given

Table 6

Activation energy ΔE and 60-min half-life temperature T of AWC800 and AWC1200

| Sample | Activation energy, ΔE (kJ mol ⁻¹) | 60-min half-life temperature, T (K) |
|---------|---|---------------------------------------|
| AWC1200 | 105.6 | 417.3 |
| AWC800 | 94.81 | 390.3 |

in Table 6, only for means to show AWC1200 show higher oxidation resistance than AWC800.

Acknowledgment

RO wishes to thank SONY Institute of Higher Education for financial support.

References

- [1] T. Okabe, K. Saito, Japanese Patent Publication A, H14-164806, 1992.
- [2] R. Ozao, T. Okabe, T. Arii, Trans. Mater. Res. Soc. Jpn. 28 (2003) 1075–1078.
- [3] R. Ozao, T. Arii, T. Okabe, D. Capogna, M. Ochiai, Trans. Mater. Res. Soc. Jpn. 29 (2004) 2435–2438.
- [4] R. Ozao, W.-P. Pan, N. Whitely, T. Okabe, Energy Fuels 18 (2004) 638–643.
- [5] R. Ozao, T. Okabe, Y. Nishimoto, Y. Cao, N. Whitely, W.-P. Pan, Energy Fuels 19 (2005) 1729–1734.
- [6] T. Okabe, K. Saito, M. Fushitani, M. Otsuka, J. Porous Mater. 2 (1996) 223–228.
- [7] M. Kano, M. Momota, T. Okabe, K. Saito, Thermochim. Acta 292 (1996) 175–177.
- [8] Y. Oishi, M. Kano, K. Morita, Y. Yamauchi, M. Morita, Mater. Trans. 44 (2003) 1163–1166.
- [9] K. Watanabe, K. Sakanishi, I. Mochida, Energy Fuels 16 (2002) 18–22.
- [10] A.K. Kercher, C. Nagle, Carbon 41 (2003) 15–27.
- [11] K. Liu, Y. Gao, J.T. Riley, W.-P. Pan, A.K. Mehta, K.K. Ho, S.R. Smith, Energy Fuels 15 (2001) 1173–1180.
- [12] S.C. Saxena, Prog. Energy Combustion Sci. 15 (1990) 55–94.
- [13] W. Hodek, M. Kramer, H. Juntgen, Fuel 70 (1990) 424–428.
- [14] Y. Chen, S. Mori, W.-P. Pan, Thermochim. Acta 275 (1996) 149–158.
- [15] W.-P. Pan, Y. Gan, M.A. Serageldin, Thermochim. Acta 180 (1991) 203–217.
- [16] Y. Chen, S. Mori, W.-P. Pan, Energy Fuels 9 (1995) 71–74.
- [17] J.V. Ibarra, R. Moliner, M.P. Gavilan, Fuel 70 (1991) 408–413.
- [18] P.R. Solomon, D.G. Hamblen, R.M. Carangelo, M.A. Serio, G.V. Deshpande, Energy Fuels 2 (1988) 405–422.
- [19] R. Cao, S. Naya, R. Artiaga, A. Garcia, A. Valera, Polym. Degrad. Stab. 85 (2004) 667–674.
- [20] J.H. Flynn, L.A. Wall, J. Polym. Sci. Part B: Polym. Lett. 4 (1966) 323–328.
- [21] T. Ozawa, Bull. Chem. Soc. Jpn. 38 (1965) 1881–1886.